Proceedings of the 21st ICSMGE, Vienna, Austria, 14 – 19 June 2026. Pistrol, Adam & Schweiger (eds.)
Published by: ÖGG, Austrian Society for Geomechanics, Salzburg, Austria, ISBN 978-3-9503898-4-5
https://doi.org/10.53243/ICSMGE2026-624

Study on the interaction characteristics between giant composite diaphragm wall foundation and soil in deep soft soil interlayer area

Qian Yin, Weiming Gong, Guoliang Dai
Southeast university, Nanjing, China; Jianghan university, Wuhan, Cina, yq1992168@163.com

Xiaojuan Li, Mingxing Zhu
Jiangsu University of Science and Technology, Zhenjiang, China

ABSTRACT: The main span of Zhangjinggao Yangtze River Bridge, a world-class super-long-span suspension bridge under construction in China, reaches 2,300 meters. The anchorage foundation of the bridge is located in the deep soft soil interlayer area. Considering the construction feasibility and bearing characteristics, a novel type of giant composite diaphragm wall foundation (CDWF) is adopted. Centrifugal model tests and numerical simulation analyses were carried out for this type of foundation, and the horizontal bearing characteristics and the interaction mechanism between the foundation and the soil were studied. The displacement characteristics, the resistance distribution law of soil, and the foundation’s failure mechanism under external load are obtained. The results show that the rotation and translational displacement of the foundation occur simultaneously when the external load is applied, and the rotation center migrates dynamically with the load. The research results provide a valuable reference for the theoretical analysis and engineering application of CDWF.

KEYWORDS: CDWF, centrifuge test, ABAQUS, foundation-soil interaction, load transfer mechanism.

1 INTRODUCTION

With the steady advancement of China's "Transportation Powerhouse" development strategy, the demand for constructing super-long-span suspension bridges has been growing rapidly. To accommodate broader waterways and higher traffic load requirements, bridge spans are gradually breaking the 2,000-meter threshold. Up to now, China has completed a series of globally representative super-long-span suspension bridges, achieving remarkable accomplishments that have attracted worldwide attention. Zhangjinggao Yangtze River Bridge[0], currently under construction with a main span of 2,300 meters, as shown in Figure 1, surpasses the current world record holder−the 2,023-meter main span of the Çanakkale Bridge in Turkey−and will set a new world record upon completion.

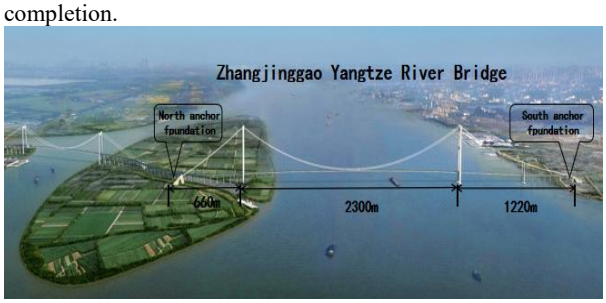

Figure 1. Visualization of Zhangjinggao Yangtze River Bridge.

Zhangjinggao Yangtze River Bridge features cable tensions as high as 140,000 tons. Located in a deep, water-rich soft soil interlayer zone with no hard bearing stratum within 150 meters[0]. Its north anchor foundation is embedded at depths ranging from −30 m to −48 m, where thick layers of silty clay interlayers are present, the geological conditions are shown in Figure 2. The design and construction of the anchor foundation for this super-long-span suspension bridge face dual challenges of intricate load distribution and poor geological conditions. Currently, the most common anchor foundation types for super-long-span suspension bridges worldwide include embedded gravity anchors, caissons, and diaphragm walls. Traditional single-type foundations, require continuous increases in structural dimensions to meet bearing demands, which in turn escalates construction costs and technical difficulties. To address these challenges, Zhangjinggao Yangtze River Bridge adopts an innovative approach by combining the construction advantages of diaphragm walls with the load-bearing benefits of caissons. The design features:

- A double-walled rectangular outer frame with grid-type inner walls to resolve construction difficulties;
- An underwater concrete sealing slab cast at the base of the inner grid walls to minimize dry excavation risks;
- The outer walls embedded into the hard bearing stratum below the foundation to form a water-cutoff curtain while transferring vertical loads.

This configuration ultimately forms a novel CDWF that integrates the diaphragm wall, embedded soil, and surrounding soil into a synergistic load-bearing system. This highly promising foundation system fully leverages the retaining, load-bearing, and waterproofing functions of diaphragm walls while optimizing soil-structure interaction. By adopting a rational structural layout, external loads are efficiently transferred to the ground, achieving optimal vertical and horizontal bearing performance.In this composite foundation, the diaphragm wall transitions from a traditional support function to a dual role of both support and structural component, effectively simplifying construction processes and enhancing resource utilization. However, its bearing mechanism currently lack established design theories, necessitating further research and innovation.

In light of this, this paper conducts an investigation into the CDWF, with particular focus on the critical issue of load transfer mechanism. By employing large-scale centrifuge model tests combined with numerical simulations, the research investigates the soil-foundation interaction mechanism of giant CDWFs. The study aims to reveal the horizontal bearing capacity and deformation characteristics of the CDWFs, thereby providing theoretical support for the optimized design and bearing performance analysis of CDWFs.

2 CENTRIFUGE TEST PROCEDURE AND RESULTS

2.1 *Test equipment*

The test setup utilized the large-scale arm centrifuge, with a capacity of 400 g·t. This centrifuge can achieve a maximum acceleration of 200g and a corresponding maximum load of 2t[0].

It is equipped with a 64-channel automated measurement system, covering measurement parameters including soil pressure, strain, and displacement. During testing, vertical loads from the upper anchor body were applied through the model anchor, while horizontal loads were exerted via servo-controlled hydraulic actuators mounted on a movable rigid frame. The horizontal loading system incorporated force and displacement sensors. The equipment are shown in Figure 3.

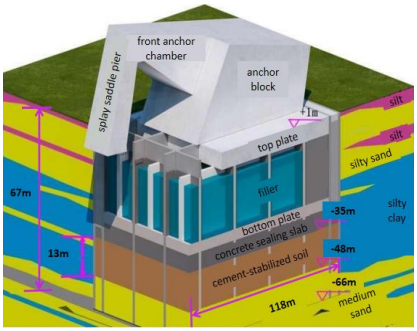

Figure 2. The north anchor foundation and its geological conditions.

Figure 3. The centrifuge and its horizontal loading equipment.

Laser displacement sensors (L) and miniature soil pressure sensors (T) were employed to capture the time variations in soil displacement and pressure during testing, respectively, as illustrated in Figure 4.

Figure 4. The displacement and soil pressure sensor.

2.2 *Test plan*

The test was based on the prototype of the north CDWF for Zhangjinggao Yangtze River Bridge, measuring 118m(L)×75m(B)×67m(D). The centrifugal acceleration was set at 160g, corresponding to a model scaling ratio of N=160. Given the longitudinal symmetry of both the model and loading conditions, a half-model along the bridge axis was designed and installed adjacent to the transparent window of the model container. The model foundation was constructed using aluminum alloy and comprised two components: The upper anchor body primarily functions to counterbalance vertical eccentric loads and transfer horizontal eccentric loads during bearing, with its dimensions determined according to load similarity criteria; The external diaphragm walls are designed to resist sectional bending moments, governed by equivalent flexural stiffness similarity criteria.The internal partition walls act as bracing elements, sized based on axial stiffness similarity principles. The schematic diagram of the prototype foundation is presented in Figure 5, and the detailed dimensional parameters of the prototype and model foundations provided in Table 1.

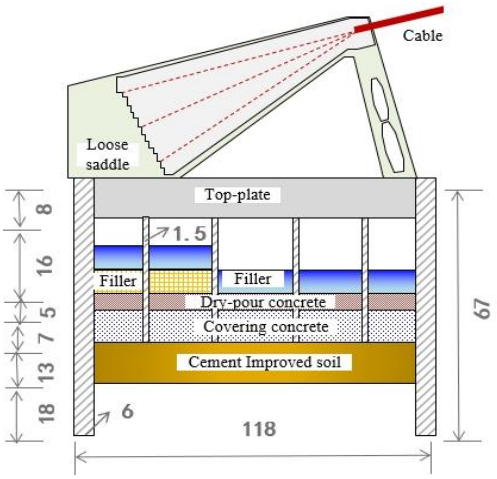

Figure 5. The schematic diagram of the prototype foundation.

Table 1. CDWF prototype and centrifuge model dimensions.

Parameter	Prototype	Half-model	Scaling ratio
Length/m	118	0.737	1:N
Breadth/m	75	0.234	1:2N
Depth/m	67	0.419	1:N
Exterior wall thickness/m	6	0.028	$(E_p/E_m)^{1/3}$:N
Foundation depth /m	37	0.231	1:N
Improved soil depth/m	50	0.313	1:N
Internal partition wall thickness/m	1.5	0.004	E_p/E_m:N

The tests were carried out under three distinct working phases based on actual engineering practices:

- Construction: Post-completion of CDWF, H_0 = 0 kN (self-weight only).
- Loading: Bridge operational state under design load, H_1 = 1.34×10^6 kN.
- Ultimate: double design load, H_2 = 2.68×10^6 kN.

The load is applied to the IP point (57m height above the top plate) indicated in Figure 5 at a uniform acceleration load rate of 0.05 kN / s.

2.3 *Test preparation*

Test soil was obtained from the construction site, consisting of silty sand, coarse sand and silty clay, with their strati-graphic distribution illustrated in Figure 6 in both model and prototype scales. To account for particle size effects in the coarse sand[0], particles larger than 13 mm were removed and equivalent substitution method was employed to determine the particle gradation. The sandy soil was then prepared using layered compaction method to achieve the target relative density. The preparation process followed a systematic layered approach: First, saturated sandy soil was compacted layer-by-layer from bottom to top until reaching the target density. Subsequently, near-saturated, flow-plastic clay prepared by water immersion and homogenization in a vacuum mixer was sequentially poured into the model container from the base upward. Before preparation, estimate the amount of clay required for the net space of the model box based on one-dimensional consolidation theory. First, pour the dried clay into a mixer, then add an appropriate amount of water. Seal the container and thoroughly stir the mixture under vacuum until uniform, preparing a slurry with a moisture content of approximately twice the liquid limit.

Pour the slurry into the model box. Under 1g conditions, apply a pressure of 50kPa to the surface of the slurry for one-dimensional pre-consolidation, with a consolidation period of 3 months. After the one-dimensional consolidation is complete, remove the pressure from the soil surface and proceed with centrifugal consolidation under 160g conditions until the degree of consolidation of the soil meets the requirements. Finally, upper layers of saturated silty sand were similarly prepared through stratified compaction.

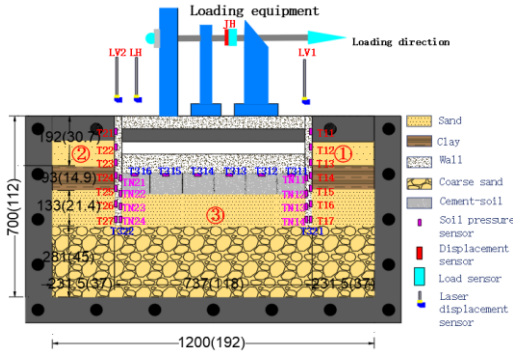

Figure 6. The schematic diagram of the model foundation.

The undrained shear strength s_u of clay measured by the micro T-bar instrument is shown in Figure 7. The test value is similar to the empirical formula given by Lai[0] and Gourvenec[0], that is, the undrained shear strength of clay is approximately linear along the depth, which has been confirmed by many scholars[00]. The soil is reinforced by P.O 42.5 ordinary portland cement, the cement content is 35 %, and the unconfined compressive strength of the 14d reaches 2.3 MPa. The elastic modulus E = 220 MPa is measured by the test[0]. The similarity ratio conversion design is carried out according to the diameter of 2.1 m, the pile length of 13 m and the replacement rate of 0.7. After the consolidation is completed, the physical and mechanical parameters of the model soil are shown in Table 2. In addition, other physical and mechanical parameters of silty clay and coarse sand particle gradation curves are given, as shown in Table 3 and Figure 8.

After the consolidation of the model soil is completed, the underground diaphragm wall trench is excavated, and the cement soil pile is excavated and installed in the base cement reinforcement area, and then the underground continuous wall foundation is installed. The whole model installation process is shown in Figure 9. The model wall is reserved with soil pressure sensor holes for laying soil pressure sensors.The schematic diagram for the layout of soil pressure and displacement sensors is shown in Figure 6, and the physical picture is shown in Figure 10.

Table 2. Physical and mechanical parameters of consolidated soil.

Soil	Thickness / m	Moisture content ω / %	Density ρ / g·cm^{-3}	Undrained shear strength S_u / kPa	Relative compaction D_r / %
Sand	30.7	24.4	1.94	/	55
Clay	14.9	32.1	1.84	60~90	/
Sand	21.4	23.4	1.93	/	60
Coarse sand	45.0	11.7	2.04	/	65

Table 3. Physical and mechanical parameters of clay.

Cohesion c_d / kPa	Angle of friction φ_d / °	Liquid limit ω_L / %	Plasticity index I_p / kPa	Coefficient of consolidation C_v / cm^2·s^{-1}	Permeability coefficient k / m·s^{-1}
12.4	33.7	37.5	14.8	8.83×10^{-3}	1.00×10^{-9}

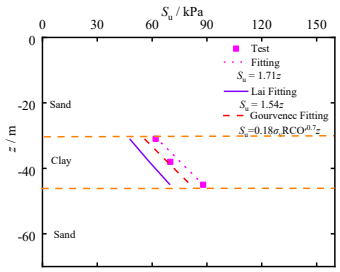

Figure 7. The undrained shear strength S_u of clay.

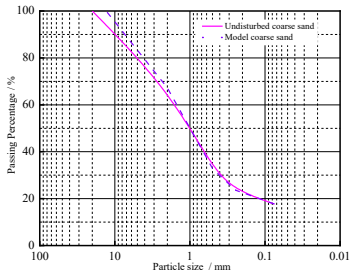

Figure 8. Coarse sand particle gradation curve.

(a) 1g soil consolidation (b) Cement-soil pile model

(c) Cement-soil pile installation (d) Model soil completion

(e) The foundation model and the anchor body

Figure 9. The preparation process of the test.

2.4 *Test procedure*

The prepared model is hoisted to the centrifuge basket, and the upper anchor body and loading equipment are installed. The test is started after the centrifuge is started to run to 160 g. After the soil stress state reaches stability, the test data are recorded to obtain the bearing characteristics of CDWF under the load H_0; After the horizontal load is applied to H_1, the acceleration remains unchanged, and the acceleration is continuously observed for a certain time. The test data are recorded to explore the bearing characteristics of CDWF under the operating load; Continue to uniformly accelerate the slow application of horizontal load to H_2 after continuous observation to the centrifuge full load operation limit time, end the test, record the test data to explore the bearing characteristics of the foundation under the ultimate load.

After the test, the physical and mechanical properties of the soil at different depths were tested during the unloading process to check the soil parameters. At the same time, the deformation characteristics of soil and foundation are observed. In order to

be able to intuitively reflect the prototype, the monitoring results of the model wall are converted into prototypes for comparison and analysis. The relevant data are collected under the stable operation of the centrifuge acceleration to 160 g.

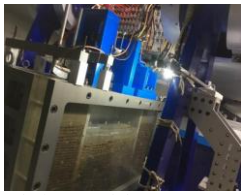

Figure 10. The physical picture of the test.

3 TEST RESULTS

3.1 *Displacement response*

The displacement curve of the north CDWF under different loading conditions is shown in Figure 11.

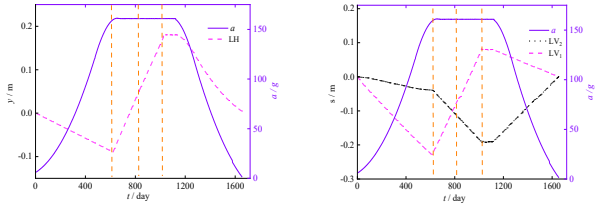

(a) Horizontal (b) Vertical

Figure 11. The displacement response of the test.

It can be seen from Figure 11 that the displacement of the foundation increases with the increase of acceleration. When the acceleration is stable to 160 g, under the action of H_0 load, the horizontal displacement y of the back wall top is backward -0.09 m and the vertical displacement s_2 is downward 0.20 m. At the same time, the vertical displacement s_1 of the front wall top is downward 0.026 m, that is, the rigid body deflection and the downward vertical settlement of the front end of the foundation. When the horizontal load is uniformly accelerated from H_0 to H_1 and H_2, the rigid body deflection of the rear end of the foundation is lifted and the front end is sunk. The horizontal displacement y increases from -0.09 m to +0.05 m and +0.018 m respectively. The vertical displacement s_2 at the top of the rear exterior wall gradually rises from 0.20 m to 0.06 m and -0.09 m. The vertical displacement s_1 at the top of the front exterior wall gradually sinks from 0.03 m to 0.10 m and 0.18 m until the load is applied, and the displacement tends to be stable.

3.2 *Soil pressure response*

The soil pressure curve of the north anchorage foundation under different working conditions is shown in Figure 12. It can be seen from the diagram that the soil pressure of the foundation increases with the increase of acceleration. In the construction stage, the soil pressure outside the back wall first increases and then decreases with depth, and the soil pressure outside the front wall gradually increases with depth. The soil pressure of the base and the bottom of the wall generally shows a trend of large at the back end and small at the front end. The reason is that the rigid body rotation of the back end sinking and front end lifting occurs. The passive and active states of soil pressure in different regions of the foundation above and below the rotation point are different. The mechanism is more complicated due to the influence of various factors such as rotation center, soil property, excess pore water pressure and displacement. When the acceleration is stable to 160 g, as the foundation displacement tends to be stable, the soil stress tends to be stable after redistribution.

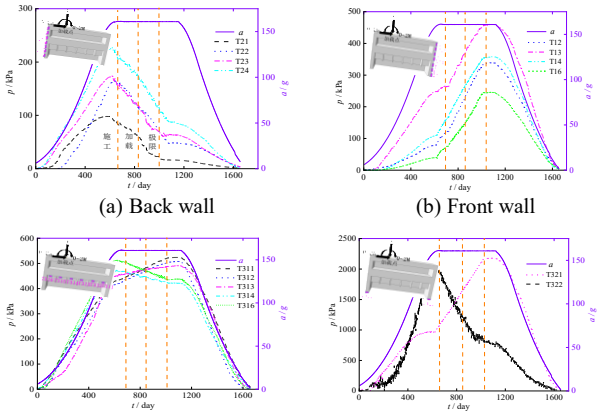

(a) Back wall (b) Front wall

(c) Base bottom (d) Wall bottom

Figure 12. The soil pressure response of the test.

3.3 *Deformation of soil*

After the test, the observation model found that the front side of the foundation sank due to rotational displacement, and the soil in the range of 20 m ahead was squeezed and uplifted, and obvious cracks could be observed on the surface of the soil. The back side of the foundation is uplifted, and the soil near the back wall and side wall of the foundation is destroyed. There are obvious ground cracks in a certain range in front of the model and at the corner. In addition, horizontal cracks at different depths can be observed from the transparent glass plate, as shown in Figure 13.

The soil in front and back of the foundation is excavated layer by layer, and the physical and mechanical parameters of the soil are measured in real time to check the soil parameters. Then, the foundation is pulled out with the hanging pile equipment. During the unloading process, it is found that the external load makes the foundation closely combine with its embedded cement soil pile and embedded soil, and become a whole to work together, as shown in Figure 14. In addition, it can also be observed that some cement-soil piles at the rear and front ends of the first compartment of the foundation are damaged. The reason why cement-soil piles in other areas are almost not damaged is that the foundation is deflected backward and forward during the construction stage and the operation stage, respectively. The soil pressure at the rear and front ends of the foundation bottom reaches the maximum in both cases, which is the most unfavorable area for bearing capacity.

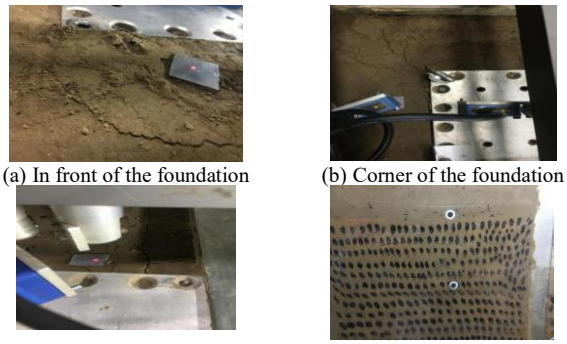

(a) In front of the foundation (b) Corner of the foundation

(c) Behind the foundation (d) Along the load direction

Figure 13. The deformation form of the soil.

Figure 14. The unloading process of the test.

4 FINITE ELEMENT ANALYSIS

In this section, a finite element model corresponding to the centrifugal test was carried out to explore the bearing mechanism of the foundation.

4.1 *Modeling and simulation process*

The model size, load action and soil boundary are the same as those of the centrifugal test, and the same stress field as the centrifugal test is realized by setting the acceleration a = 160 g. The boundary conditions are: the left and right sides of the model box are constrained in the X direction, the front and rear sides are constrained in the Y direction, and the bottom is constrained in the X, Y, and Z directions. The foundation and soil are composed of C3D8. The sensitivity analysis shows that the grid division method can ensure the calculation accuracy and model convergence. Numerical simulation of the three-dimensional model and meshing are shown in Figure 15.

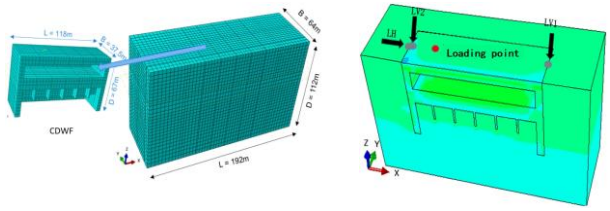

Figure 15. The finite element model and its displacement extraction points

In order to facilitate the comparative analysis of the later results, the numerical simulation models in this chapter are described and analyzed according to the N = 160 conversion as the prototype size. The displacement extraction points of the model are set according to the displacement meter layout points in the centrifugal test scheme. As shown in Figure 15.

The Coulomb friction model is employed to account for the nonlinear behavior of the contact interface. A surface-to-surface contact scheme is adopted, with normal behavior defined as hard contact to allow for both slip and separation at the interface. Tangential behavior is characterized by defining a friction coefficient to reflect the frictional properties and roughness of the contact surfaces. The friction coefficient was set to 0.37 based on values obtained from laboratory tests[0]. The influence of the installation process of the foundation on the test is not considered. Firstly, the initial in-situ stress balance analysis of the soil is carried out, and then the soil excavated by the foundation construction is set to the failure state through the Model Change birth and death unit. At the same time, the foundation and the foundation-soil contact surface unit are activated, and then the horizontal loads of three working conditions are applied on the top surface of the foundation. In order to avoid the stress concentration at the loading point, the coupling constraint is adopted between the loading point and the top surface of the foundation.

4.2 *Model material properties*

The foundation material is aluminum alloy, and the linear elastic model is adopted. The elastic modulus E = 70 GPa and the Poisson 's ratio v = 0.3. The elastic-plastic Mohr-Coulomb model is used for soil. From Figure 7, it can be seen that the strength of silty clay increases approximately linearly with depth. According to the proportional relationship between the Young 's modulus E of soil and S_u[0], the Young 's modulus of soil E in this paper is E/S_u = 1500. The linear relationship between the elastic modulus E of sand and the intermediate principal stress is $E = \kappa p_{at} (\sigma_m/p_{at})^{\lambda}$, where p_{at} = 100 kPa; κ and λ are two dimensionless coefficients, which are 400 ~ 600 and 0.55~0.6 in medium dense sand and dense sand, respectively[0].

In order to ensure the validity of the numerical simulation analysis, the elastic modulus E varying with depth is defined by the user-defined subroutine USDFLD. The elastic modulus parameters of cement reinforced soil are taken as E = 220 MPa. The internal friction angle and cohesion are taken as the recommended values in Reference[0]. The values of soil parameters are shown in Table 4.

Table 4. Physical and mechanical properties of finite element soil.

Soil	Thickness / m	Effective unit weight γ' / kN·m^{-3}	Cohesion c / kPa	Angle of friction φ / °	Poisson ratio v
Sand	30.7	10.0	/	33	0.30
Clay	14.9		13	32	0.35
Sand	21.4		/	35	0.30
Coarse sand	45.0		/	38	0.30
Cement-soil	13		1000	33	0.25

4.3 *Analysis result*

Figure 16 shows the displacement comparison results of the centrifugal test and finite element analysis model of the north anchor. It can be found from the figure that the horizontal and vertical displacements of the foundation increase with the increase of load. In the construction stage, the eccentric self-weight of the anchor body leads to the backward deflection of the foundation, and the horizontal displacement of the foundation decreases linearly from the top to the bottom. At the same time, the back end of the foundation sinks and the front end rises, and the vertical displacement gradually decreases linearly from the back wall to the front wall. With the increase of the horizontal load, the foundation is deflected from the back to the front, the horizontal displacement is gradually changed from the back to the front, the back wall is lifted upward and the front wall is sunk downward. The foundation is inclined and deformed under the load, which proves that the foundation is rigid. The horizontal bearing capacity usually depends on the horizontal displacement allowed by the superstructure of the foundation.

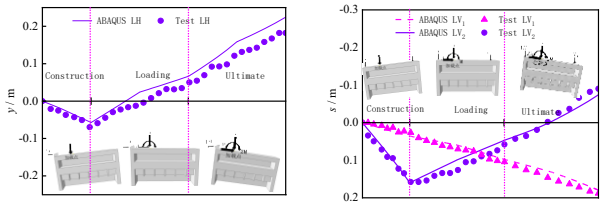

(a) Horizontal (b) Vertical

Figure 16. The displacement comparison results.

Figure 17 shows the soil pressure comparison results of the centrifugal test and finite element analysis model of the north anchor. It can be found from the figures that the displacement and soil pressure values of the centrifugal test and the finite element analysis model are not much different, which verifies that the bearing characteristics of the finite element model analysis foundation are more reasonable and credible.

Figure 18 shows the displacement cloud diagram and vector diagram obtained by the finite element model analysis of different working conditions. From the diagram, it can be found that when the horizontal load is H_0, the foundation rotation center is located at the 2/3D buried depth position on the front side of the foundation; as the horizontal load gradually increases to H_1, the foundation rotates forward, and the rotation center of the foundation is located at the D buried depth on the outer and back sides of the foundation when the load is completed. As the horizontal load further increases to H_2, the foundation continues to rotate forward. When the load is completed, the rotation center of the foundation gradually shifts

forward, and finally shifts to the position where the foundation is buried deep D and 1/3L away from the back outer wall. The rotation center migrates dynamically with the change of load. The reason is that the horizontal load is small, the foundation only mobilizes the surrounding shallow soil to resist the external load, the rotation center is located within the buried depth of the foundation, and the left and right positions are related to the direction of load action. When the horizontal load gradually becomes larger, the eccentric self-weight of the foundation will offset part of the external load. Finally, the effect of the external load of the foundation is greater than the effect of the eccentric self-weight, so the forward deflection occurs. The rotation center of the foundation gradually approaches the foundation and shifts downward, mobilizing more and more soil to participate in resisting the load effect.

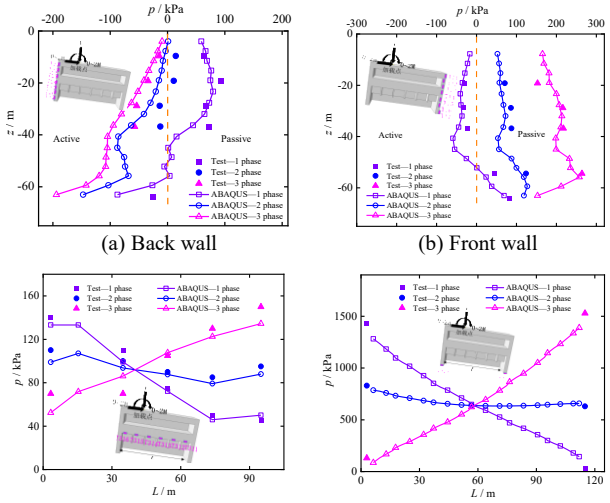

(a) Back wall (b) Front wall

(c) Base bottom (d) Wall bottom

Figure 17. The soil pressure comparison results.

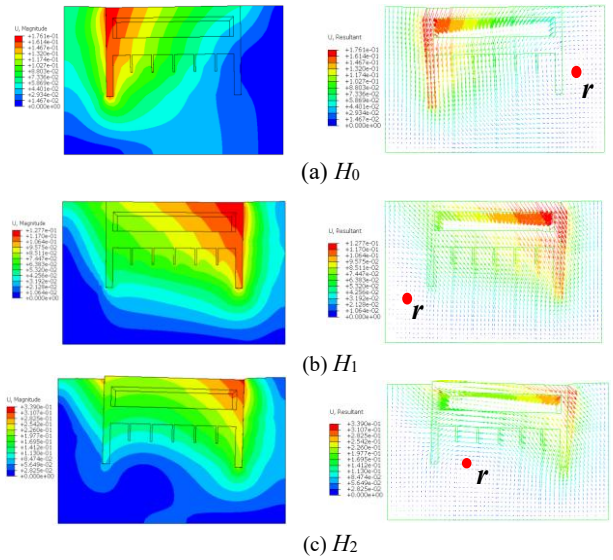

(a) H_0

(b) H_1

(c) H_2

Figure 18. The displacement cloud and vector diagram.

5 CONCLUSIONS

Based on the north CDWF of Zhangjinggao Yangtze River Bridge, centrifugal test and finite element analysis are carried out for the horizontal bearing capacity of the foundation. The main conclusions are as follows :

- The foundation occurs in the backward deflection of the back-end sinking and the front-end lifting in the construction stage, and the forward deflection of the front-end sinking in the back-end lifting in the operation stage. In the whole loading project, the foundation displacement increases slowly until the load is applied, and the displacement tends to be stable.
- The distribution curve of soil pressure on the outer side of the front and rear walls of the foundation roughly shows that the passive zone increases first and then decreases with depth, and increases with the increase of horizontal load. The active zone increases with the increase of depth and decreases with the increase of horizontal load. The soil pressure of the basement and the bottom of the wall generally shows a trend of large sinking end and small lifting end. The distribution curve of soil pressure in different regions of the foundation is affected by many factors, such as rotation center, soil property, and displacement, and the mechanism is more complicated.
- Under the action of external load, the displacement of the foundation causes the soil in front of the foundation to be squeezed and uplifted, and the soil near the back wall and side wall of the foundation is damaged by traction. Obvious ground fissures are generated in a certain range and at different depths in front of the model and at the corner. The foundation and its embedded soil are closely combined to play a role as a whole. The bottom of the front and rear ends of the foundation is the most unfavorable area for bearing.
- The results of displacement and soil pressure measured by centrifugal test are in good agreement with the numerical simulation results, and the rotation center of the foundation migrates dynamically with the change of load. The smaller the load and the stronger the bearing capacity of the foundation, the more backward and downward the rotation center moves. The larger the load and the weaker the bearing capacity of the foundation, the more forward and upward the rotation center moves.

6 REFERENCES

CCCC Highway Consultants Co., Ltd., 2021. Preliminary design of Zhangjinggao Yangtze River crossing project, Beijing, China.

Wang N. X., Zhang W. M. 2015. Geotechnical centrifuge modeling technology and applications, China.

Lai Y. Q., Wang L. Z., Hong Y., et al. 2020. Centrifuge modeling of the cyclic lateral behavior of large-diameter monopiles in soft clay: effect of episodic cycling and re-consolidation. Ocean Eng., 200, 107048.

Gourvenec S, Acosta-artinez H E, Randolph M, 2009. Experimental study of uplift resistance of shallow skirted foundations in clay under transient and sustained concentric loading. Géotechnique,59(6): 525-537.

Dyvik R., Andersen K. H., Hansen S. B., et al. 1993. Field tests of anchors in clay I: Description. J. Geotech. Eng., 119(10), 1515-1531.

Reese L., Cox W., Koop F. 1975. Field testing and analysis of laterally loaded piles om stiff clay. Paper presented at the Offshore Technology Conference, Houston, Texas.

Yin Q. 2025. Lateral bearing capacity of composite diaphragm wall anchor foundation. Southeast University, China.

Peng S. K. 2024. Research on horizontal bearing characteristics of multi chamber diaphragm wall anchorage foundation in soft soil. Southeast University, China.

Li G. X. 2004. Advanced Soil Mechanics, China.

Wang Y. 2022. Study on size effect and cyclic bearing capacity of large diameter lateral loaded piles in sandy soil. Southeast University, China.

Han J., Ye G., B., Ye S., L. 1994. Ground Treatment and Underpinning Technology, China.